Dalton Transactions

ROYAL SOCIETY OF CHEMISTRY

COMMUNICATION

View Article Online
View Journal | View Issue

Cite this: *Dalton Trans.*, 2022, **51**, 4246

Received 6th January 2022,
Accepted 18th February 2022

DOI: 10.1039/d2dt00055e

rsc.li/dalton

Gas-phase deposition of di- and tetra-lithium salts of 2,5-dihydroxyterephthalic acid†

Juho Heiska [a,b] and Maarit Karppinen *[a]

Thin films of two ambipolar lithium-organic electrode materials, Li_2DHTP and Li_4DHTP, are grown from gaseous precursors, Li(thd) (tetramethyl heptanedione) and DHTP (dihydroxyterephthalic acid). These precursors are pulsed into the reactor in a sequential manner like in atomic/molecular layer deposition, but the reaction product, *i.e.* the di- or the tetra-lithium salt, is controlled by adjusting the precursor pulse lengths.

Introduction

Metal salts of 2,5-dihydroxyterephthalic acid (H_4-DHTP) comprise an interesting group of coordination polymer (CP) and metal–organic framework (MOF) type metal–organic materials with extraordinarily rich coordination chemistries.[1–5] The richness arises from the two different reactive groups, carboxylic acid, and phenol, both present as duplicates in the H_4-DHTP molecule. This allows the formation of both di- and tetra-metal salts, depending on the bonding scheme and the degree of deprotonation of H_4-DHTP. A comprehensive account of the coordination modes with different metals is found in a recent paper by Quarez *et al.*[6] Potential applications proposed for these materials include gas adsorption, detection, and separation,[2,4,5,7,8] as well as active rechargeable batteries[3,9,10] and electrochromic devices.[11]

With lithium, both the H_4-DHTP derivatives, Li_2DHTP and Li_4DHTP (Fig. 1), have been realized in crystalline form through conventional solution-synthesis routes, using respectively, Li_2CO_3 or MeOLi as the lithium source.[3,9,10] The Li-rich Li_4DHTP is air-sensitive though, yielding Li_2O as a result of auto-oxidation.[3] The carboxylate moiety undergoes reversible redox reactions at *ca.* 0.8 V *vs.* Li^+/Li and the aryloxide (reacted phenol) at *ca.* 2.6 V *vs.* Li^+/Li. This makes Li_4DHTP – similarly to Na_4DHTP[12] – an interesting ambipolar electrode material for symmetric cells with an average working potential of 1.8 V *vs.* Li^+/Li.[9]

Electrochemically active organic materials, in general, are currently gaining significant attention. They may not beat the state-of-the-art inorganic electrode materials in overall battery performance but could provide an attractive alternative when issues related to critical raw materials, energy-efficient synthesis/recycling, or gravimetric and mechanical properties are considered. The major challenges of the organic electrode materials are their intrinsically low electron conductivity and dissolution in liquid electrolytes; these issues can, however, be circumvented by applying the materials in thin-film form in combination with a solid electrolyte.[13–17] The all-solid-state thin-film configuration would also serve as an optimal model system for investigating the intrinsic properties of organic electrode materials and understanding their solid-state electrochemical behavior and stability.[15,18–22] Hence, it is important to develop reliable and scalable thin-film fabrication processes for the most interesting organic electrode materials.

In recent years, the combined ALD/MLD technique,[23–25] derived from the atomic layer deposition (ALD) technology of high-quality inorganic thin films for microelectronics and beyond, has been harnessed for the growth of many intriguing *in situ* crystalline metal–organic materials directly from gaseous precursors.[18–20,26–32] A prototype ALD process is based on two mutually reactive gaseous (or evaporated with moderate

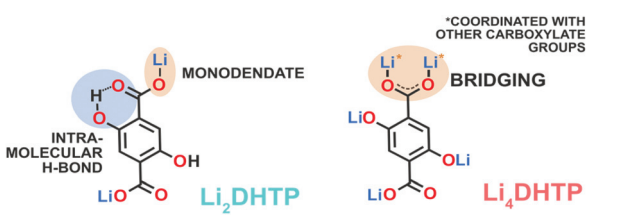

Fig. 1 Visualization of the chemical compositions and specific bonding features of the targeted materials.

[a]*Department of Chemistry and Materials Science, Aalto University, FI-00076 Espoo, Finland. E-mail: maarit.karppinen@aalto.fi*
[b]*Vaasa University of Applied Sciences, Energy & Environmental Technology, FI-65200 Vaasa, Finland*

†Electronic supplementary information (ESI) available. See DOI: 10.1039/d2dt00055e

heating) precursors sequentially pulsed into the reactor chamber to facilitate the atomic layer by atomic layer film growth with excellent control for the film thickness, homogeneity, and conformity. Ideally, the two successive surface reactions should saturate and be self-limiting, meaning that the growth per cycle (GPC) levels of to a constant value when long enough precursor pulses are applied. Molecular layer deposition (MLD) is an extension of ALD, to deposit purely organic thin films from two different organic precursors in a similar fashion; ideally, the process controllability and the film quality should be of the same level as in ALD. Then, in the hybrid ALD/MLD technique a metal-bearing ALD precursor is combined with an organic MLD precursor to deposit metal–organic thin films within the same sequential gas–surface reaction scheme. The precursor pulse times required for perfect saturation are somewhat reactor and reaction condition specific, but usually these pulsing times do not exceed a few seconds for metal precursors and a few tens of seconds for heavy organic precursors (longer pulse lengths needed due to their typically lower vapor pressures).[24,33–35]

In this communication, we use a similar sequential precursor supply scheme to introduce Li(thd) (thd = 2,2,6,6-tetramethyl-3,5-heptanedione) and H_4-DHTP precursor vapors in an ALD/MLD reactor chamber. Excitingly, the films grow in a highly reproducible manner such that the film thickness is well controlled by the number of ALD/MLD cycles applied (once the other deposition parameters are fixed), but the end product, *i.e.* Li_2DHTP or Li_4DHTP, depends on the lengths of the precursor pulses. The two types of films are readily distinguished from each other with X-ray diffraction, infrared absorption, and cyclic voltammetry data.

Methods

Commercial H_4-DHTP powder (98%, Sigma-Aldrich) and in-house synthesized Li(thd) powder were used as the precursors; the reagents for Li(thd) synthesis were LiOH (98%, Alfa Aesar) and 2,2,6,6-tetramethyl-3,5-heptanedione (Tokyo Chemical Industry Co. Ltd) and the product was purified by sublimation. The films were grown on p-doped silicon test wafers (Okmetic Ltd), and also on stainless steel disks (MTI Corporation) for the electrochemical characterization, using an F-120 flow-type hot-wall ALD reactor (ASM Microchemistry Ltd) functioning at a low pressure of *ca.* 5 mbar and operated under nitrogen (99.999%) atmosphere generated from the air (Parker HPN 5000 N_2 generator). The same N_2 gas was used as a carrier and purge gas. The Li(thd) and H_4-DHTP precursor powders, placed in separate containers within the reactor, were heated for sublimation at 175 and 190 °C, respectively; the latter temperature was chosen based on TG-vacuum analysis.[36] Most of the depositions were made at 200 °C, but few depositions of 300 cycles were made at 250 °C, just to confirm that the observations also take place at higher temperatures.

The X-ray diffraction patterns were recorded for the samples in grazing-incidence geometry (GIXRD; X'Pert Pro, PANalytical; Cu Kα; incidence angle 0.5°). X-ray reflectivity (XRR) patterns were recorded with the same equipment to determine the film thicknesses and densities. Chemical compositions and bonding structures were studied with Fourier transform infrared spectroscopy (FTIR; Bruker Alpha II); the resolution was 4 cm^{-1} over 32 scans, and the spectrum of a blank reference wafer was subtracted from the measured spectra.

Samples for the electrochemical characterizations were deposited on stainless steel substrates (∅ 15.5 mm). These coated steel disks were applied as a working electrode in CR2016 coin cells assembled in a glove box (<1 ppm of O_2 and <0.1 ppm of H_2O). The samples were dried in a vacuum (110 °C) and moved under vacuum into a glovebox (<1 ppm for O_2, <0.1 ppm for H_2O). Lithium foil (Sigma Alrdich, 99.9%) was used as a counter electrode, and 1 M $LiPF_6$ in 1 : 1 EC : DMC as electrolyte. The cells were let to stabilize for 24 hours prior to the cyclic voltammetry (CV) measurements (Autolab PGSTA302N potentiostat).

Results

Since H_4-DHTP contains both carboxylic acid and phenol functional groups, we could expect from our previous experiences with terephthalic acid and hydroquinone precursors combined with Li(thd) and LiHMDS (lithium bis(trimethylsilyl)amide), respectively,[18,19,37] that H_4-DHTP could readily react with these common lithium precursors; for the present study, our choice was Li(thd), but presumably, LiHMDS would work similarly. Based on these previous experiences, we selected the following precursor and purge pulsing sequence for our initial experiments: 4 s Li(thd)/4 s N_2/10 s H_4-DHTP/30 s N_2. As was predicted, this process was found to yield Li-organic thin films in a reproducible manner independent of the pulsing sequence. Further analysis with GIXRD and FTIR (details discussed later) indicated that the films were *in situ* crystalline of the Li_2DHTP phase.

Among the two types of functional groups, the carboxylic acid group is more acidic, and our assumption was that it would react first with Li(thd); indeed, this seems to be the case as the deposition product was found to be Li_2DHTP. Then, the exciting discovery was that apparently the reaction proceeds further to Li_4DHTP if the Li(thd) pulse length is elongated. When the Li(thd) pulse length exceeded 32 s (while keeping the H_4-DHTP pulse length fixed at 10 s, the crystalline films were found to transform into amorphous Li_4DHTP phase. This second reaction step resulting in Li_4DHTP was noticed – besides the GIXRD observation – from the GPC *versus* Li(thd) pulse length plot in Fig. 2, as this plot does not show the ordinary saturation behavior expected for a prototype ALD/MLD process yielding a single product. From Fig. 2, essentially phase-pure Li_2DHTP films could be grown with the rate of *ca.* 4–8 Å per cycle, while the GPC value seen in the case of the essentially phase-pure Li_4DHTP films was *ca.* 13 Å per cycle, *i.e.* roughly twice the value seen for Li_2DHTP. It should

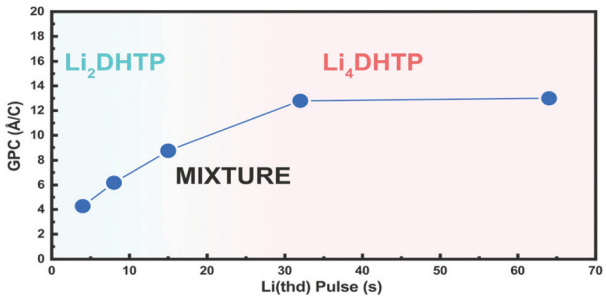

Fig. 2 GPC *versus* Li(thd) pulse length (H_4-DHTP pulse length fixed to 10 s); the resultant product (Li_2DHTP or Li_4DHTP) is highlighted.

however be noted that compared to the Li_2DHTP films, the Li_4DHTP films were less uniform with some thickness profile along the flow direction, and thus the GPC values were less precise.

The two phases, Li_2DHTP and Li_4DHTP, present in the samples were most easily distinguished by FTIR (Fig. 3a). In both cases, the features seen in the spectra can be interpreted based on the spectra previously reported and interpreted for bulk Li_2DHTP to Li_4DHTP samples (ESI S1–3†).[3,10] The most important features are the asymmetric (ν_{as}) and symmetric (ν_s) vibrations of the carboxylate group. The separation of these vibrations gives a rough indication of the binding mode between the metal ion and the carboxylate group. The transformation from Li_2DHTP to Li_4DHTP decreases the peak separation from 281 to 193 cm^{-1} and shifts the position of the ν_{as} peak from 1642 to 1557 cm^{-1}. The straightforward interpretation of these observations would be that the binding mode changes from monodentate for Li_2DHTP to bridging type for Li_4DHTP.[38] The coordination chemistry of DHTP is however quite complicated, and verification of this interpretation would require knowledge of the detailed crystal structure which unfortunately is known for neither Li_2DHTP nor Li_4DHTP. Indeed, only the crystal structure of hydrated Li_2DHTP·$4H_2O$ is known,[6] but this structure is apparently different from those of Li_2DHTP and Li_4DHTP judging from their different XRD patterns. An additional important signature to distinguish Li_4DHTP from Li_2DHTP in FTIR is the wide absorption feature seen for Li_2DHTP in the 2500–3000 cm^{-1} area due to intramolecular hydrogen bonding between the phenol and carbonyl groups. These peaks are naturally not seen for Li_4DHTP, as such hydrogen bonds are not possible.

The phase composition of the films was visible also from the XRR and GIXRD data (Fig. 3b and c). The film densities derived from the XRR data were different for the films composed of Li_2DHTP (1.73 g cm^{-3}) and Li_4DHTP (1.52 g cm^{-3}). From GIXRD, the Li_2DHTP films are well crystalline, with very intense peaks at 27.6° and 28.6°; the intensity ratio and peak positions match the previously reported diffraction pattern for evacuated bulk samples of Li_2DHTP (but not those of Li_2DHTP·$4H_2O$,[6] as already mentioned).[10] The as-deposited Li_4DHTP films were amorphous, but were crystallized in ambient conditions over the night, forming – most likely – the quinone variant (no phenol groups) of Li_2DHTP, and eventually – unless protected – Li_2O as reported earlier for bulk samples.[3] In contrast to Li_4DHTP, the Li_2DHTP films were stable in ambient conditions, and did not absorb moisture.

We characterized the electrochemical properties of the Li_2DHTP and Li_4DHTP films with cyclic voltammetry measurements (Fig. 4). Firstly, for Li_2DHTP cycled between 1.5–3.5 V,

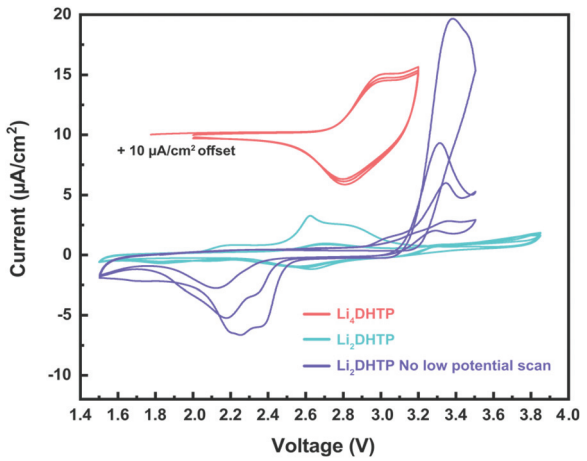

Fig. 4 Cyclic voltammograms for Li_2DHTP and Li_4DHTP films. The Li_4DHTP voltammogram is offset by 10 μA cm^{-2}.

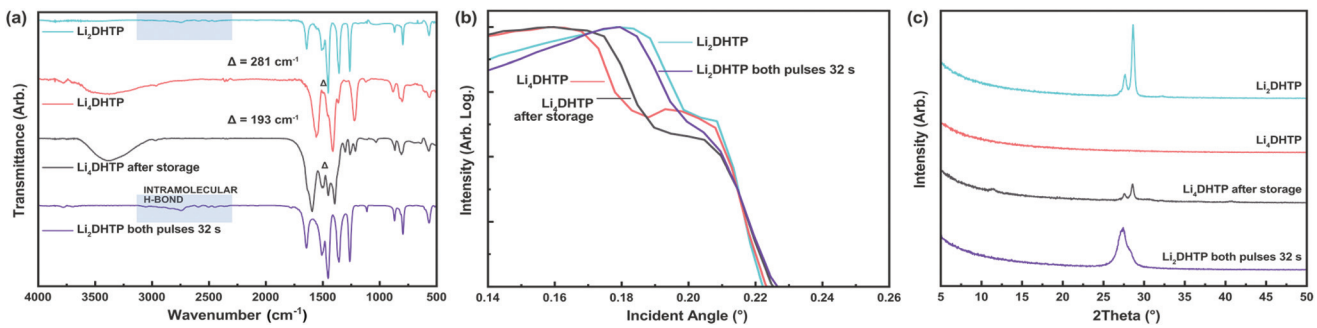

Fig. 3 Representative (a) FTIR spectra (most important spectral features highlighted), (b) XRR patterns, and (c) GIXRD patterns to show the differences between the Li_2DHTP and Li_4DHTP films.

no electrochemical activity due to the alkoxide/quinone pair was observed; the irreversible peaks seen are probably due to the electrochemical activity of the phenol (–OH).[39] It is known that phenol groups can be lithiated at low potentials coupled with formation of H_2 gas.[40–42] Here also, the Li_2DHTP film could be electrochemically lithiated into Li_4DHTP by sweeping the potential to 0.1 V and back to OCV. After this lithiation cycle the alkoxide/quinone redox pair appeared at *ca.* 2.6 V *vs.* Li^+/Li, as expected.[3,9] The as-grown amorphous Li_4DHTP film behaved in a different fashion; it exhibited only a single redox pair centered around 2.9 V (and unstable behaviour at higher voltages), which does not exactly agree with the expected quinone redox pair value. Whether or not this peak is due to some other redox pair in the molecule remained to be clarified in more detailed studies in the future. However, here we like to refer to a somewhat similar case of ALD V_2O_5 films, grown in both crystalline and amorphous forms depending on the precursors used, and showing different electrochemical characteristics depending on the crystalline/amorphous nature of the films.[43] Finally, we should mention that among the two phases, Li_2DHTP and Li_4DHTP, the latter is preferred for the electrochemical applications, as it possesses the required functional groups both for the negative (–COOLi) and the positive (–OLi) electrode redox couples. Moreover, in this compound the phenol groups are already lithiated such that no H_2 is formed during the cell operation.

Discussion

To gain a deeper understanding of the surface chemistry features of our Li(thd) + H_4-DHTP deposition process, we carried out a set of additional experiments with different combinations of precursor pulse lengths (Table S1†). The clear conclusion was that essentially phase pure (crystalline) Li_2DHTP films are reproducibly obtained when the Li(thd) pulse length is short and also clearly shorter than that of H_4-DHTP. On the other hand, to deposit pure (amorphous) Li_4DHTP films the Li(thd) pulse needs to be considerably longer than that of H_4-DHTP. When the H_4-DHTP pulse length was of the same magnitude as that of Li(thd), the GPC value became very high (exceeding even 30 Å per cycle when the pulse length was 32 s for both precursors); it should be noted, however, that the film thickness determination was somewhat ambiguous for the films with the highest GPC values due to their roughness.

Tentatively, we assume that the Li_4DHTP phase forms through a similar lithium-replacing reaction as is known to occur for the transformation of MgF_2 to LiF.[44] Hence, intuitively one might think that an efficient method to fabricate Li_4DHTP could be to lithiate Li_2DHTP just with a very long Li(thd) pulse at the end of the film growth process. However, in practice, this may not work as pure Li_2DHTP is difficult to form in the given conditions. This is further explained below.

In Fig. 5 we present a schematic illustration of the reaction process. In **phase 1**, the faster reaction between Li(thd) and the carboxylic acid group takes place forming initially Li_2DHTP. After this, Li_2DHTP lays on the surface and if the incoming Li(thd) pulse is long enough, the lithiation of the phenyl moiety also begins, to eventually form Li_4DHTP in **phase 2**. Most likely this second reaction step is less controlled than the first one, being thus the underlying reason why the Li_4DHTP films were less uniform than the Li_2DHTP films. In **phase 3**, the formed Li_4DHTP reacts with the incoming H_4-DHTP precursor; here again, the carboxylic acid group reacts more readily than the phenyl group with the –OLi group. This reaction converts one Li_4DHTP moiety into two Li_2DHTP moieties, which can again react in the "expected" way with the H_4-DHTP precursor. The proposed surface reac-

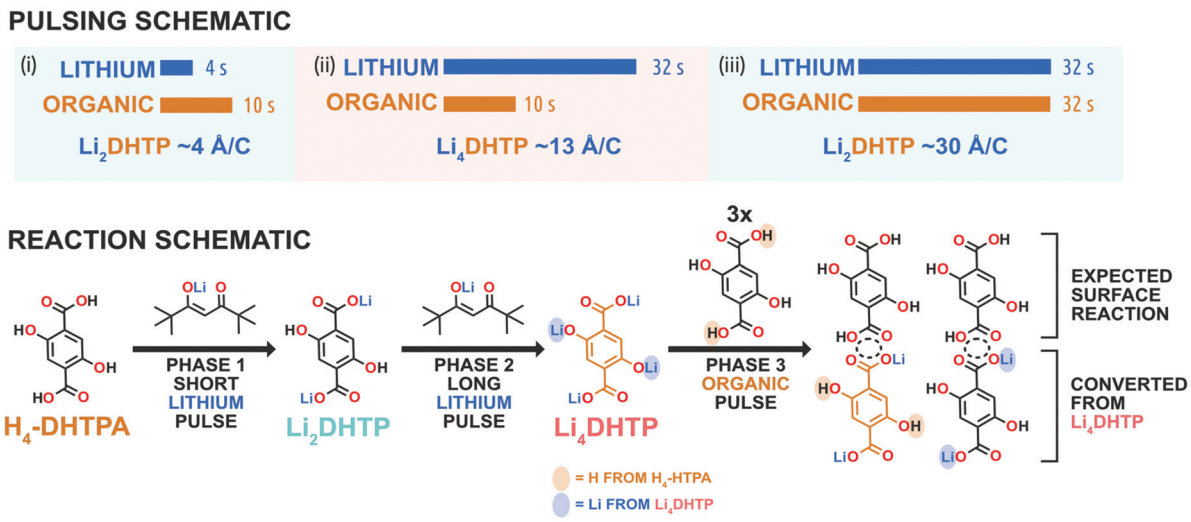

Fig. 5 Schematic illustration of the proposed reactions occurring in the Li(thd) + H_4-DHTP process with different precursor pulse lengths.

tions could be simplified with the following exchange reactions:

$$2\mathrm{Li(thd)\ (ads)} + \mathrm{H_4\text{-}DHTP\ (g)} \rightarrow \mathrm{Li_2DHTP\ (s)} + 2\mathrm{H(thd)\ (g)}$$

$$\mathrm{Li_2DHTP\ (s)} + 2\mathrm{Li(thd)\ (g)} \rightarrow \mathrm{Li_4DHTP\ (s)} + 2\mathrm{H(thd)\ (g)}$$

$$\mathrm{Li_4DHTP\ (s)} + \mathrm{H_4\text{-}DHTP\ (g)} \rightarrow 2\mathrm{Li_2DHTP\ (s)}$$

$$2\mathrm{Li_2DHTP\,(s)} + 2\mathrm{H_4\text{-}DHTP\,(g)} \rightarrow 2\mathrm{Li_2DHTP\,(s)} + 2\mathrm{H_4\text{-}DHTP\,(ads)}$$

Owing to the exchange of H_4-DHTP to Li_4DHTP, during one cycle four H_4-DHTP moieties may be deposited on the surface. Thus, to make the deposition process for Li_2DHTP films as controllable as possible, the formation of Li_4DHTP during the process should be avoided, as its transformation back to Li_2DHTP leaves extra molecules on the surface.

The Li_4DHTP films, on the other hand, often exhibited gradients over areas where the precursor flux is expected to be the highest; the most straightforwardly expected cause for this is an insufficient precursor pulse time. It seems that Li_4DHTP forms fastest on the substrate areas that saturate first. If the whole film area is not successfully converted into Li_4DHTP, large growth gradients may quickly form due to the extra surface species generated (that would again saturate quicker than the other areas making the problem even worse).

Finally, we like to mention that in principle, it should be possible to perfectly transform the entire film into Li_4DHTP and then back to Li_2DHTP to achieve uniform Li_2DHTP coatings with an extraordinarily high growth rate. However, this was difficult to achieve in practice and the experiments resulted in non-uniform growth along the flow direction. In the future, it might be interesting to play with the reactivity of the lithium precursor. Towards this research direction, we already carried out a few experiments with LiHMDS that is more reactive than Li(thd), to find out that the growth rate increased but the film uniformity got worsened. The other option, *i.e.* to look for a less reactive lithium precursor, remained to be challenged in future works.

Conclusions

We have presented straightforward and reproducible gas-phase fabrication routes for two intriguing Li-organic materials, Li_2DHTP and Li_4DHTP, for the first time. The processes are based on two precursors only, *i.e.* Li(thd) and H_4-DHTP, sequentially pulsed in an ALD/MLD type reactor. The exciting feature – which distinguishes the processes from the ideal ALD/MLD scheme – is that the phase composition of the films is controlled by the precursor pulse lengths, the Li_2DHTP films requiring shorter and the Li_4DHTP films longer Li(thd) pulses. The Li(thd) + H_4-DHTP process delivers the Li_2DHTP films in *in situ* crystalline form, while the Li_4DHTP films are initially amorphous but are crystallized during storage in ambient conditions. Preliminary characterization of the films with cyclic voltammetry experiments demonstrated that both the Li_2DHTP and Li_4DHTP films are electrochemically active, as desired.

We foresee that similar unconventional surface-reaction pathways as found and successfully utilized here for the Li_2DHTP and Li_4DHTP films could be innovatively exploited also with other interesting organic molecules with multiple different reactive groups connected to the same organic moiety.

Author contributions

Juho Heiska: Conceptualization, methodology, investigation, writing – original draft, visualization. Maarit Karppinen: Supervision, funding acquisition, writing – original Draft.

Conflicts of interest

There are no conflicts of interest to declare.

Acknowledgements

Funding was received from the Academy of Finland (Profi 3 and PREIN) for this study which also made use of RawMatTERS Finland Infrastructure (Aalto – RAMI).

Notes and references

1 J. De Bellis, D. Belli Dell'Amico, G. Ciancaleoni, L. Labella, F. Marchetti and S. Samaritani, *Inorg. Chim. Acta*, 2019, **495**, 118937.
2 R. Sanz, F. Martínez, G. Orcajo, L. Wojtas and D. Briones, *Dalton Trans.*, 2013, **42**, 2392–2398.
3 S. Renault, S. Gottis, A.-L. Barrès, M. Courty, O. Chauvet, F. Dolhem and P. Poizot, *Energy Environ. Sci.*, 2013, **6**, 2124.
4 S. R. Caskey, A. G. Wong-Foy and A. J. Matzger, *J. Am. Chem. Soc.*, 2008, **130**, 10870–10871.
5 H. Chun and D. Moon, *Cryst. Growth Des.*, 2017, **17**, 2140–2146.
6 É. Quarez, A. Jouhara, S. Grolleau, F. Dolhem, N. Dupré and P. Poizot, *CrystEngComm*, 2020, **22**, 1653–1663.
7 B. Li, H.-M. Wen, W. Zhou and B. Chen, *J. Phys. Chem. Lett.*, 2014, **5**, 3468–3479.
8 Y. Lv, T. Xu, P. Xu, H. Yu and X. Li, in 2017 19th International Conference on Solid-State Sensors, Actuators and Microsystems (TRANSDUCERS), IEEE, 2017, pp. 303–306.
9 S. Wang, L. Wang, K. Zhang, Z. Zhu, Z. Tao and J. Chen, *Nano Lett.*, 2013, **13**, 4404–4409.
10 Q. Deng, J. Xue, W. Zou, L. Wang, A. Zhou and J. Li, *J. Electroanal. Chem.*, 2016, **761**, 74–79.
11 H. Shiozawa, Z. Melnikova, Z. Bastl, H. Peterlik, M. Kalbac and O. Frank, *ChemRxiv.*, 2021, 1–17.
12 S. Wang, L. Wang, Z. Zhu, Z. Hu, Q. Zhao and J. Chen, *Angew. Chem., Int. Ed.*, 2014, **53**, 5892–5896.

13 P. Poizot, J. Gaubicher, S. Renault, L. Dubois, Y. Liang and Y. Yao, *Chem. Rev.*, 2020, **120**, 6490–6557.
14 B. Häupler, A. Wild and U. S. Schubert, *Adv. Energy Mater.*, 2015, **5**, 1402034.
15 J. Heiska, M. Nisula and M. Karppinen, *J. Mater. Chem. A*, 2019, **7**, 18735–18758.
16 Y. Liang and Y. Yao, *Joule*, 2018, **2**, 1690–1706.
17 Y. Lu and J. Chen, *Nat. Rev. Chem.*, 2020, **4**, 127–142.
18 J. Heiska, M. Nisula, E.-L. Rautama, A. J. Karttunen and M. Karppinen, *Dalton Trans.*, 2020, **49**, 1591–1599.
19 M. Nisula and M. Karppinen, *Nano Lett.*, 2016, **16**, 1276–1281.
20 J. Multia, J. Heiska, A. Khayyami and M. Karppinen, *ACS Appl. Mater. Interfaces*, 2020, **12**, 41557–41566.
21 J. Kint, F. Mattelaer, M. Minjauw, B. Zhao and C. Detavernier, *J. Vac. Sci. Technol., A*, 2019, **37**, 050904.
22 B. Zhao, M. Nisula, A. Dhara, L. Henderick, F. Mattelaer, J. Dendooven and C. Detavernier, *Adv. Mater. Interfaces*, 2020, **7**, 2001022.
23 P. Sundberg and M. Karppinen, *Beilstein J. Nanotechnol.*, 2014, **5**, 1104–1136.
24 S. M. George, *Chem. Rev.*, 2010, **110**, 111–131.
25 O. Nilsen, K. Klepper, H. Nielsen and H. Fjellvåg, *ECS Trans.*, 2008, **16**, 3–14.
26 J. Penttinen, M. Nisula and M. Karppinen, *Chem. – Eur. J.*, 2019, **25**, 11466–11473.
27 J. Penttinen, M. Nisula and M. Karppinen, *Chem. – Eur. J.*, 2017, **23**, 18225–18231.
28 A. Khayyami, A. Philip and M. Karppinen, *Angew. Chem., Int. Ed.*, 2019, **58**, 13400–13404.
29 E. Ahvenniemi and M. Karppinen, *Chem. Commun.*, 2016, **52**, 1139–1142.
30 O. Nilsen, V. Miikkulainen, K. B. Gandrud, E. Østreng, A. Ruud and H. Fjellvåg, *Phys. Status Solidi*, 2014, **211**, 357–367.
31 H. H. Sønsteby, J. E. Bratvold, V. A.-L. K. Killi, D. Choudhury, J. W. Elam, H. Fjellvåg and O. Nilsen, *J. Vac. Sci. Technol., A*, 2020, **38**, 060804.
32 M. Madadi, J. Heiska, J. Multia and M. Karppinen, *ACS Appl. Mater. Interfaces*, 2021, **13**, 56793–56811.
33 A. S. Asundi, J. A. Raiford and S. F. Bent, *ACS Energy Lett.*, 2019, **4**, 908–925.
34 R. W. Johnson, A. Hultqvist and S. F. Bent, *Mater. Today*, 2014, **17**, 236–246.
35 V. Cremers, R. L. Puurunen and J. Dendooven, *Appl. Phys. Rev.*, 2019, **6**, 021302.
36 J. Multia, A. Khayyami, J. Heiska and M. Karppinen, *J. Vac. Sci. Technol., A*, 2020, **38**, 052406.
37 M. Nisula, J. Linnera, A. J. Karttunen and M. Karppinen, *Chem. – Eur. J.*, 2017, **23**, 2988–2992.
38 V. Zeleňák, Z. Vargová and K. Györyová, *Spectrochim. Acta, Part A*, 2007, **66**, 262–272.
39 E. S. Gil and R. O. Couto, *Rev. Bras. Farmacogn.*, 2013, **23**, 542–558.
40 S. Goriparti, M. N. K. Harish and S. Sampath, *Chem. Commun.*, 2013, **49**, 7234.
41 J. Lee and M. J. Park, *Adv. Energy Mater.*, 2017, **7**, 1602279.
42 C. Wang, W. Tang, Z. Yao, Y. Chen, J. Pei and C. Fan, *Org. Electron.*, 2018, **62**, 536–541.
43 X. Chen, E. Pomerantseva, K. Gregorczyk, R. Ghodssi and G. Rubloff, *RSC Adv.*, 2013, **3**, 4294.
44 M. Mäntymäki, J. Hämäläinen, E. Puukilainen, T. Sajavaara, M. Ritala and M. Leskelä, *Chem. Mater.*, 2013, **25**, 1656–1663.